THE JOURNAL OF PHYSICAL CHEMISTRY A

Article

pubs.acs.org/JPCA

# Solvent-Induced Luminescence Quenching: Static and Time-Resolved X-Ray Absorption Spectroscopy of a Copper(I) Phenanthroline Complex

T. J. Penfold,[†,‡,§] S. Karlsson,[†] G. Capano,[†,‡] F. A. Lima,[†,⊥] J. Rittmann,[†] M. Reinhard,[†] M. H. Rittmann-Frank,[†] O. Braem,[†] E. Baranoff,[∥] R. Abela,[§] I. Tavernelli,[‡] U. Rothlisberger,[‡] C. J. Milne,[†,#] and M. Chergui*[,†]

[†]Laboratoire De Spectroscopie Ultrarapide and [‡]Laboratoire De Chimie Et Biochimie Computationnelles, École Polytechnique Fédérale De Lausanne, ISIC, FSB-BSP, CH-1015 Lausanne, Switzerland

[§]SwissFEL, Paul Scherrer Inst, CH-5232 Villigen, Switzerland

[∥]School of Chemistry, University of Birmingham, Edgbaston, Birmingham, B15 2TT, United Kingdom

Supporting Information

**ABSTRACT:** We present a static and picosecond X-ray absorption study at the Cu K-edge of bis(2,9-dimethyl-1,10-phenanthroline)-copper(I) ($[Cu(dmp)_2]^+$; dmp = 2,9-dimethyl-1,10-phenanthroline) dissolved in acetonitrile and dichloromethane. The steady-state photoluminescence spectra in dichloromethane and acetonitrile are also presented and show a shift to longer wavelengths for the latter, which points to a stronger stabilization of the excited complex. The fine structure features of the static and transient X-ray spectra allow an unambiguous assignment of the electronic and geometric structure of the molecule in both its ground and excited $^3$MLCT states. Importantly, the transient spectra are remarkably similar for both solvents, and the spectral changes can be rationalized using the optimized ground- and excited-state structures of the complex. The proposed assignment of the lifetime shortening of the excited state in donor solvents (acetonitrile) to a metal-centered exciplex is not corroborated here. Molecular dynamics simulations confirm the lack of complexation; however, in both solvents the molecules come close to the metal but undergo rapid exchange with the bulk. The shortening of the lifetime of the title complex and nine additional related complexes can be rationalized by the decrease in the $^3$MLCT energy. Deviations from this trend may be explained by means of the effects of the dihedral angle between the ligand planes, the solvent, and the $^3$MLCT-$^1$MLCT energy gap.

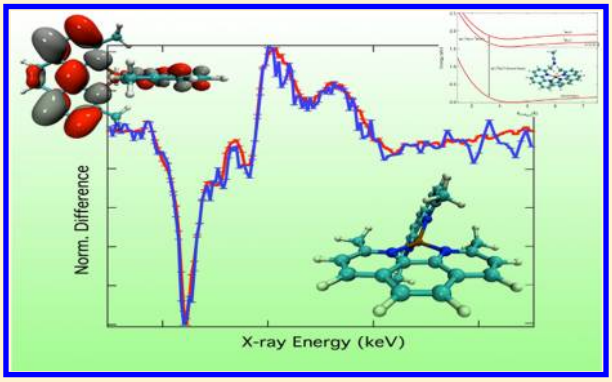


## INTRODUCTION

The role of the solvent in driving, hindering, or modifying the outcome of reactions is of fundamental importance for chemistry. With the advent of ultrafast spectroscopy, a wide range of studies, typically in the optical or infrared spectral ranges, have been carried out aimed at describing the initial solvent response for the simplest unimolecular process, a photoinduced charge redistribution in the solute.[1−3] These studies of solvation dynamics have delivered, with the help of molecular dynamics (MD) simulations, detailed insight into the mechanistic aspects of the solvent rearrangements; however, they are not capable of retrieving the structure of the solvation shell.

In contrast, the study of the solvent structure around small, typically atomic solutes in the ground state has been performed for several decades using static X-ray absorption spectroscopy (XAS) and X-ray scattering,[4] which can directly deliver bond distances and coordination numbers of the solvation shell. In particular for XAS, the X-ray absorption near-edge structure (XANES) and extended X-ray absorption fine structure (EXAFS) features are probes of the local structure around the solute, while the pre-edge features correspond to atomic transitions from the core levels of the absorbing atom to the valence orbitals and, as a consequence, they contain rich information about the electronic structure of the solute. Recent progress in this area has culminated in the advent of time-resolved XAS with pico- and femtosecond temporal resolution,[5−8] making it possible to probe the solvent response with structural sensitivity on the sub-picosecond time scale.[9]

For larger molecules, the XA spectrum of a fully coordinated atom will, in general, not show a solvent effect, even if its photophysical and photochemical properties are solvent-

Received: April 16, 2013
Revised: April 20, 2013
Published: April 25, 2013

  

dependent. This is because the XAS spectral features are dominated by the influence of the ligands and any changes to the valence and continuum wave functions induced by the solvent will not dramatically alter the transition probability with the core levels, as might be expected for valence spectroscopy. In addition, the disordered solvent will have a Debye−Waller factor much larger than that of the ligands, further reducing its influence. In contrast, for peripheral atoms, the XAS spectrum should exhibit signatures of the solvent environment because they are directly exposed to the latter. This was clear in our recent study of a rhenium carbonyl diimine complex, where the Re $L_3$-edge exhibited no solvent effect, while in contrast for the Br K-edge a clear solvent dependence was observed because the Br ligand is directly exposed to the environment.[10] A similar effect was also recently reported for a diplatinum complex using quantum mechanics/molecular mechanics (QM/MM) MD simulations.[11]

Photoexcitation can induce structural changes in a molecule such that some of its atoms may become exposed to the solvent. A case in point, much discussed in the literature, are the Cu-phenanthroline complexes,[12−16] and, in particular, bis(2,9-dimethyl-1,10-phenanthroline)copper(I) ($[Cu(dmp)_2]^+$; dmp = 2,9-dimethyl-1,10-phenanthroline). In the ground state (Figure 1a), this complex adopts a pseudotetrahedral geometry with the two ligands being orthogonal.[17] Upon excitation into the lowest singlet metal-to-ligand-charge-transfer (MLCT) state, the oxidation state of copper becomes Cu(II), and a flattening of the complex (Figure 1b) occurs because the copper $d^9$ electronic configuration is susceptible to Jahn−Teller distortions. Using ultrafast absorption and emission spectroscopy, Chen et al.[18,19] and Tahara et al.[20,21] reported that for excitation of the $^1$MLCT states of $[Cu(dmp)_2]^+$ the lowest $^3$MLCT state is populated in ∼8 ps, subsequent to fast internal conversion (IC) and intersystem crossing (ISC). Although these studies demonstrated that the solvent has little effect on the early time dynamics, McMillin and coworkers reported, following extensive characterization,[12] that the emission lifetime (summarized in Tables 1 and S1) is significantly shortened in donating solvents (i.e., those behaving as Lewis bases), such as acetonitrile (MeCN) (∼2 ns), ethylene glycol,[18] or tetrahydrofuran (<10 ns),[22] compared with nondonating solvents, such as dichloromethane (DCM) and toluene, for which the lifetime is ∼100 ns.[23] They attributed this quenching to complexation of a solvent molecule to $[Cu(dmp)_2]^+$ that most likely occurs at the metal center. The interaction between the Cu(II) atom and the electron-rich donor molecule is thought to stabilize the excited state relative to the ground state, reducing the energy gap and therefore increasing the rate of nonradiative decay.[24] This would imply that the redder the emission, the shorter the lifetime, a trend that seemed verified in the case of $[Cu(dmp)_2]^+$. Further supporting these conclusions were studies on some related complexes with bulkier ligands (see Table 1 and Figure S8 in the Supporting Information (SI)), which are supposed to prevent exciplex formation[22,25,26] and therefore reduce the quenching of the luminescence. However, these trends are far from clear in terms of donating solvents or emission wavelength. In particular, complexes such as $[Cu(phen)_2]^+$ and $[Cu(detp)_2]^+$ exhibit even shorter lifetimes in the tens of picoseconds in MeCN and hundreds of picoseconds in DCM.[27] Although $[Cu(detp)_2]^+$ has bulkier ligands, its shortened lifetime was still attributed to complexation at the metal atom by Chen et al.[28] In addition, $[Cu(dbp)_2]^+$ exhibits a lifetime

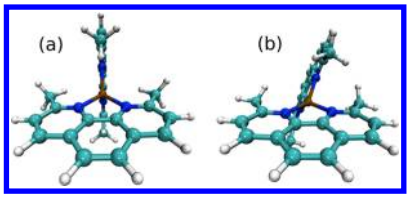


**Figure 1.** DFT (B3LYP)-optimized geometry of the ground state (a) and lowest triplet state (b) of $[Cu(dmp)_2]^+$.

**Table 1. Room-Temperature Solvent-Dependent Excited-State Lifetimes ($\tau$) and Emission Wavelengths of a Series of Cu−Phenanthroline Complexes[a]**

| | acetonitrile | | dichloromethane | | tetrahydrofuran | |
|---|---|---|---|---|---|---|
| complex | $\tau$ (ns) | $\lambda_{max}^{em}$ (nm) | $\tau$ (ns) | $\lambda_{max}^{em}$ (nm) | $\tau$ (ns) | $\lambda_{max}^{em}$ (nm) |
| $[Cu(dmp)_2]^+$ | 1.6[b] | 700[c] | 90[c] | 690[c] | <10[d,c] | 700[c] |
| $[Cu(dnpp)_2]^+$ | 100[c] | 685[c] | 260[c] | 665[c] | 140[c] | 675[c] |
| $[Cu(dpp)_2]^+$ | 120[e] | 740[e] | 270[e] | 720[e] | 190[e] | 730[e] |
| $[Cu(tfp)_2]^+$ | | | 165[f] | | | |
| $[Cu(dmdp)_2]^+$ | | | 80[f] | | | |
| $[Cu(dbp)_2]^+$ | 35[c] (35[e]) | 690[c] (730[e]) | 150[c] (150[e]) | 670[c] (715[e]) | 50[c] (50[e]) | 680[c] (725[e]) |
| $[Cu(dbtmp)_2]^+$ | 440[e] | 690[e] | 920[e] | 670[e] | 630[e] | 670[e] |
| $[Cu(tpp)_2]^+$ | | | 230[g] | 745[g] | | |
| $[Cu(dpdmp)_2]^+$ | | | 310[e] | 720[e] | | |
| $[Cu(dbdmp)_2]^+$ | | | 145[e] | 710[e] | | |
| $[Cu(dptmp)_2]^+$ | 260[e] | 735[e] | 480[e] | 715[e] | 350[e] | 725[e] |
| $[Cu(detp)_2]^+$ | 0.014[h] | | 0.20[h] | | | |
| $[Cu(phen)_2]^+$ | 0.016[h] | | 0.14[h] | | | |
| | $\varepsilon$ | DN[i] | $\varepsilon$ | DN[i] | $\varepsilon$ | DN[i] |
| | 35.70 | 14 | 8.93 | 1 | 7.43 | 20 |

[a]Dielectric constant ($\varepsilon$) and the donor number (DN); that is, the quantitative measure of Lewis basicity of the solvents. The ligand structures are shown in Figure S8 in the SI. All measurements were performed at room temperature and used the PF6 counterion. [b]Ref 18 [c]Ref 22 [d]Lifetime of $[Cu(dmp)_2]^+$ in tetrahydrofuran has not been directly measured because, like acetonitrile, it is significantly quenched. The value quoted is an upper limit based on the temporal resolution of the experimental apparatus used in ref 22. [e]Ref 25 [f]Ref 15 [g]Ref 30 [h]Ref 28 [i]kcal mol$^{-1}$.


dx.doi.org/10.1021/jp403751m | J. Phys. Chem. A 2013, 117, 4591−4601

shortening of a factor of five in donating solvents, while $[Cu(dbtmp)_2]^+$, which has the same ligands in the important 2,9 positions (Figures S8 and S9), exhibits a much smaller quenching.

To verify the hypothesis of exciplex formation, Chen et al.[19,32] used picosecond Cu K-edge XAS to investigate the excited-state structure of $[Cu(dmp)_2]^+$ in acetonitrile and toluene. Prior to this, it had been shown that the 1s → 4p feature of the Cu K-edge spectrum is a sensitive probe of the coordination.[33] In fact, for normalized spectra, this transition is expected to be approximately twice as large in tetracoordinated complexes compared with pentacoordinated ones. Chen et al. observed such a loss of intensity for the excited complex and concluded that the Cu atom was pentacoordinated in both MeCN and toluene. In later studies,[34,35] the same authors modeled the exciplex structure to fit the ground-state and transient XANES spectra. They reported that the best fit of the excited state spectrum is obtained for a model including one MeCN molecule coordinated to the copper. The nitrogen of this MeCN was only 2.0 Å from the copper atom, which places it closer than the nitrogens of the phenanthroline ligands and points to the formation of a strong exciplex at the metal center, expected to live the lifetime of the excited state. Despite this, the XAS spectra in refs 19 and 32 appear remarkably similar for both solvents, and a DFT geometry optimization of $[Cu(dmp)_2]^+\cdots$HCN reported that the acetonitrile nitrogen is more than 3.0 Å away from the copper.[19]

Thus, there is so far no clear evidence that an exciplex is formed at the metal center. Therefore, in this work we present and analyze the steady-state optical spectra of $[Cu(dmp)_2]^+$ in MeCN and DCM and also its steady-state and picosecond X-ray absorption spectra. Because of the recently implemented high repetition rate scheme for picosecond XAS,[36] we achieve a high signal-to-noise ratio that reveals fine details of the excited-state structure. We provide a concise and detailed description of the electronic and molecular structure using the finite difference method near-edge structure (FDMNES) approach[37] and time-dependent density functional theory (TD-DFT) adapted for core-hole excitations[38−40] to assign the features in the pre-edge and XANES region. We also investigate the influence of the solvent on the excited complex using classical molecular dynamics (CMD) and QM/MM MD simulations.[41−43] Our experimental results and their analysis do not support the hypothesis of exciplex formation at the metal center. Rather we conclude that the lifetime shortening is related to a relatively weak interaction between the solvent and metal complex. As a consequence of the magnitude of the interaction, this solvent molecule close to the metal rapidly exchanges between the first solvation shell and the bulk. Despite its weak nature, this interaction reduces on average the energy gap between the ground and $^3$MLCT states but also with the lowest $^1$MLCT, influencing the amount of spin mixing between these two states and therefore the emission quantum efficiency from the $^3$MLCT state.

The experimental procedure for the static and picosecond XAS experiments has already been described in refs 36 and 44 and is presented, along with the computational details, in the SI.

## EXPERIMENTAL RESULTS

**Steady-State Optical Luminescence.** Figure 2 shows the steady-state absorption and emission spectra of $[Cu(dmp)_2]^+$ in MeCN and DCM. The absorption spectrum exhibits, as

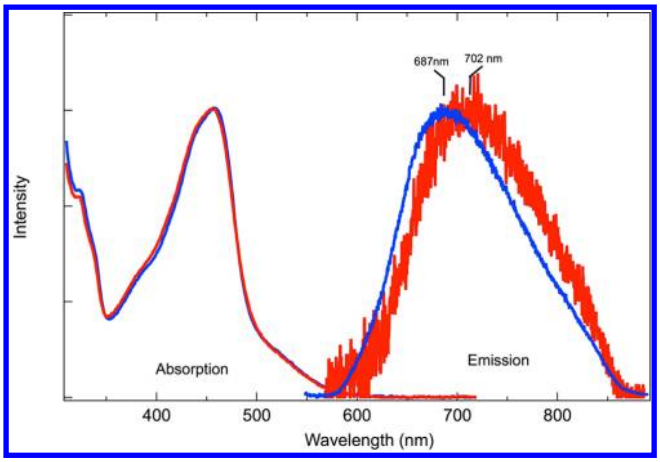


**Figure 2.** Normalized steady-state absorption and emission spectra of $[Cu(dmp)_2]^+$ dissolved in MeCN (red) and DCM (blue).

previously reported,[18,21] a main peak around 450 nm, corresponding to the $S_0 \rightarrow S_3$ transition, and a shoulder at longer wavelengths corresponding to the $S_0 \rightarrow S_1$ and $S_2$ transitions.[17] The spectra for the two solvents are almost identical with the spectrum in MeCN being slightly blue-shifted with respect to that in DCM.

The emission spectra exhibit one principal band centered around 700 nm due to emission from the $^3$MLCT state. In addition, emission from the $^1$MLCT state weakly contributes at slightly shorter wavelengths[45] but is indistinguishable from the primary $^3$MLCT emission. The spectra exhibit a ∼15 nm (∼40 meV) shift to longer wavelengths in MeCN compared with DCM, in agreement with ref 45. This shift is relatively small, considering the two-order magnitude reduction of the photoluminescence lifetime,[12−14] but it does point to a better solvent stabilization of the $^3$MLCT state in MeCN compared with DCM.

**Static and Picosecond X-ray Absorption Spectroscopy.** Figure 3a (black line) shows the edge region of the Cu K-edge absorption spectrum of the complex in acetonitrile, with features labeled A−D. The complete spectrum is shown in Figure S1 in the SI. The XANES region closely resembles that reported by Chen et al.,[19] who assigned the B band to the 1s→4p transition, based on ref 33. The weak feature, labeled A, which appears just below 8.98 keV, was also observed by Chen et al.[19,32] but was not attributed. The C and D features are above the ionization potential (IP) and are therefore multiple scattering structural features.

The transient signal in MeCN at a time delay of 50 ps for $[Cu(dmp)_2]^+$ solvated is also shown in Figure 3a. It reflects a number of distinct changes between the ground and excited states of the complex. In particular, a weak positive feature appears at 8.976 keV, which was previously assigned to a quadrupole 1s→3d transition into the hole in the highest occupied molecular orbital (HOMO) created by photoexcitation.[32] At higher energies there are strong negative and positive features in the region of the A to D features. The transient signals in MeCN and DCM are very similar, as can be seen in Figure 3b, and, importantly, the loss of intensity of the B band, which was previously taken as evidence of exciplex formation,[19,32] is identical in MeCN (red) and DCM (blue). Below, we demonstrate that this intensity loss can be interpreted in terms of the oxidation shift and can therefore not be due to pentacoordination of the metal atom. This is


dx.doi.org/10.1021/jp403751m | J. Phys. Chem. A 2013, 117, 4591−4601

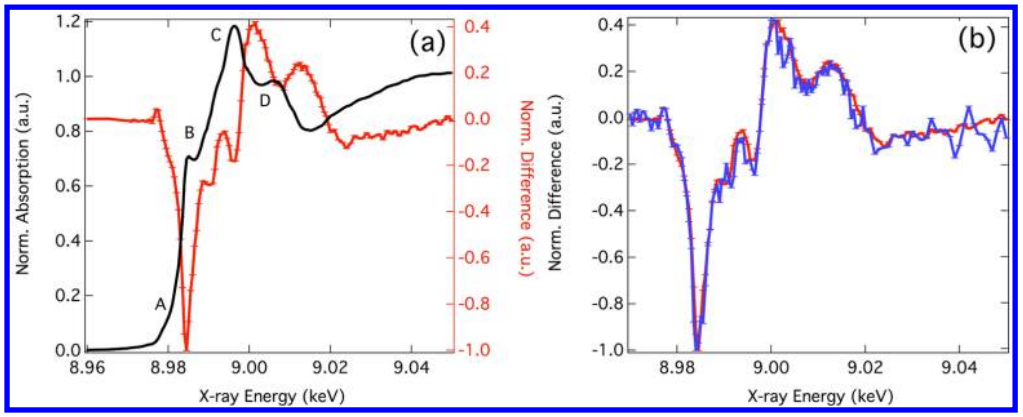


**Figure 3.** (a) Static (black) and transient (red, at 50 ps) Cu K-edge XANES spectra of $[Cu(dmp)_2]^+$ in acetonitrile. (b) Transient XANES spectrum (at 50 ps) of $[Cu(dmp)_2]^+$ in acetonitrile (red) and dichloromethane (blue). In all cases the transient spectra have been normalized to the largest difference.

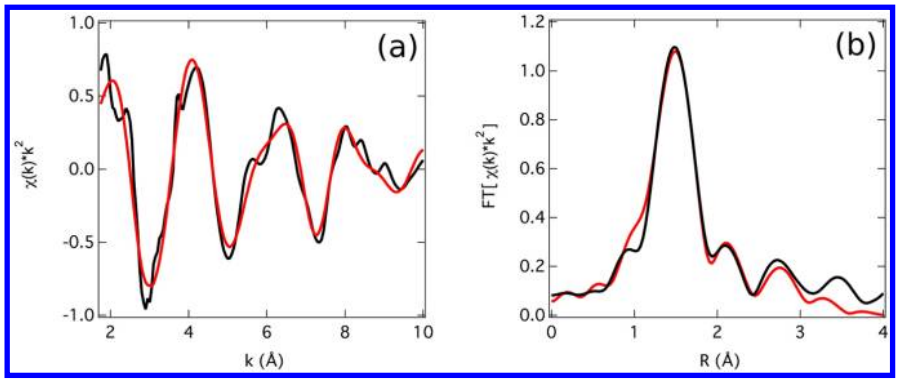


**Figure 4.** (a) Experimental (black) and simulated (red) $\chi(k)$ spectra weighted by $k^2$ (b) and associated pseudoradial distribution function of $[Cu(dmp)_2]^+$ in acetonitrile. The $k$-space range shown corresponds to the energy range of 9.01 to 9.37 keV.

confirmed later in the analysis of the transient spectra. Time scans of the largest transient feature (8.985 keV) for both MeCN and DCM are presented in Figure S2 in the SI. They show that the excited-state lifetimes for both solvents agree with the optical kinetic studies of the $^3$MLCT state.[19] In addition, Figure S3 in the SI shows that the transient spectra in MeCN at 50 ps and 1 ns are identical and therefore no significant structural changes around the metal occur in this time window.

## ■ ANALYSIS OF THE SPECTRUM

In the following sections, we will analyze the molecular and electronic structure of the ground state before moving to the analysis of the transient X-ray absorption features. Finally, we present classical and QM/MM MD simulations that shed light on the solvent's structural dynamics and its role in quenching the luminescence lifetime.

**Ground State.** *Molecular Structure.* We used the DFT (B3LYP)-derived geometry of ground state $[Cu(dmp)_2]^+$ and optimized the structure to fit the EXAFS spectrum using the IFEFFIT package.[46] The model includes eight fitting parameters: the amplitude reduction factor ($S_0^2$), the IP ($E_0$), $\Delta R_{Cu-N}$, $\Delta R_{Cu-C1}$, $\Delta R_{Cu-C2}$, $\sigma^2_{Cu-N}$, $\sigma^2_{Cu-C1}$, and $\sigma^2_{Cu-C2}$. $\Delta R_{x-y}$ denotes the distance changes of the single scattering paths from the Cu to the closest carbons and nitrogens with respect to the starting geometry. $\sigma^2_{x-y}$ denotes the variance of the scattering path length.

The experimental and best-fit EXAFS spectra, in both $k$- and $R$-space, are shown in Figure 4. The values for $E_0$ and $S_0^2$ extracted from the fit are −1.0 (±2.7) eV and 0.72 (±0.21), respectively. These parameters have large uncertainties that are generally encountered when many correlated scattering paths of similar distances contribute to the same region in $R$ space. Table 2 summarizes the results of the EXAFS analysis, as well as those from the DFT and QM/MM calculations. It shows that the Cu−N bond length is 2.03 Å, close to the value from X-ray crystallography.[47,48]

This structure can be further assessed by simulating the resonances in the XANES region of the spectrum. Figure 5 compares the experimental XANES spectrum with the

**Table 2. Structural Parameters of $[Cu(dmp)_2]^+$ in Both the Ground and $^3$MLCT States Extracted from the Methods Presented Herein[a]**

| | | DFT | EXAFS fit | | QM/MM |
|---|---|---|---|---|---|
| | | $R$ (Å) | $R$ (Å) | $\sigma^2$ (Å$^2$) | $R$ (Å) |
| Cu−N (Å) | GS | 2.09 | 2.03 | 0.02 | 2.04 ± 0.08 |
| | $^3$MLCT | 2.01 | | | 2.01 ± 0.08 |
| | | ∠ (deg) | ∠ (deg) | | ∠ (deg) |
| N−Cu−N (deg) | GS | 81.27 | 83.67 | | 83.50 ± 2.77 |
| | $^3$MLCT | 83.17 | | | 84.31 ± 2.59 |
| dmp-Cu-dmp | GS | 89.75 | 89.75 | | 88.9 ± 6.64 |
| | $^3$MLCT | 71.44 | | | 69.2 ± 7.9 |

[a]Angles were fixed because the EXAFS region is not sensitive to angles.


dx.doi.org/10.1021/jp403751m | J. Phys. Chem. A 2013, 117, 4591−4601

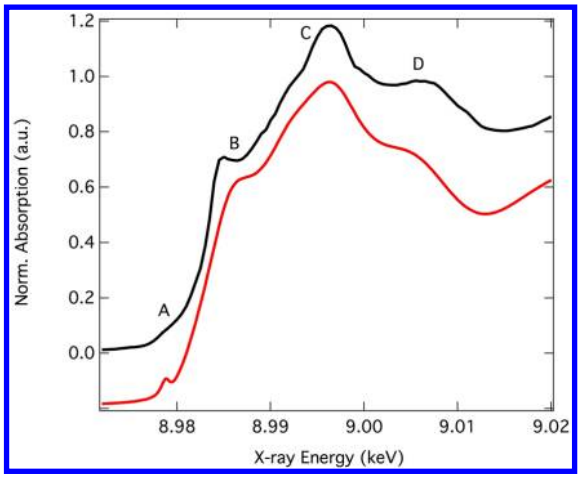


**Figure 5.** Experimental (black) and simulated using FDMNES (red) XANES spectrum for the ground state of $[Cu(dmp)_2]^+$.

absorption cross section calculated using a free form potential solved by the finite difference method within the FDMNES package.[37] The latter reproduces all of the features of the experimental spectrum and is in good agreement with the calculations of ref 34. Further understanding of the XANES resonances, which becomes important for the analysis of the transient spectrum, is provided by a shell-by-shell simulation[49] that consists of gradually increasing the number of atoms in the complex around the copper atom. The results are shown in Figure S4 in the SI, and they show that the C resonance (~8.995 keV) is already present when including only the copper, nitrogens, and closest carbon atoms into the simulation, demonstrating that it is not strongly influenced by the entire ligand environment. In contrast, the A and D features require the latter to be complete. The B feature (~8.985 keV), which plays a central role in the transient spectrum, is clearly visible upon addition of the second shell; however, its position is red-shifted when including the full ligand, in agreement with the analysis of Kau et al.[33]

*Electronic Structure.* We now investigate the electronic structure of the complex in the pre-edge and edge regions using TD-DFT adapted for core-hole excitations, as described in the SI. Figure 6 zooms into the edge region of the spectrum, with

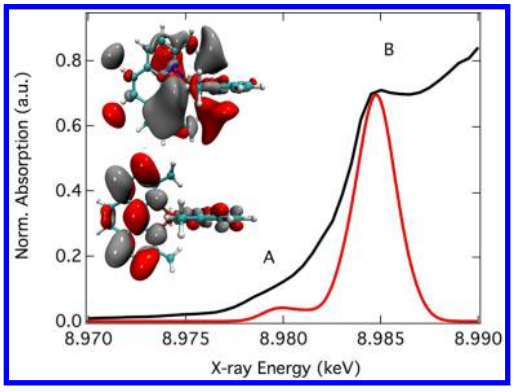


**Figure 6.** Pre-edge region of the spectrum (black) and the calculated spectrum using TD-DFT (red) with a 1.89 eV Lorentzian broadening (see Tables S2 and S3). Inset are the molecular orbitals for the transition with the largest oscillator strengths for two features. The calculated spectrum has been shifted by 5.5 eV to match the experimental spectrum.

the features labeled A and B, corresponding to those of Figure 3a. The simulated spectrum is shown in red. It has been shifted by 5.5 eV to match the experiment and broadened with a Lorentzian function of 1.89 eV width to account for the core-hole lifetime.[50]

Overall, the agreement between the two spectra is good. Tables S2 and S3 in the SI, which highlights the excitation character (i.e., the sum of singly excited determinants) of the relevant states, shows that the A feature is dominated by transitions into the lowest unoccupied molecular orbital (LUMO) and LUMO+1 orbitals. These, for which the LUMO is shown in the lower inset in Figure 6, are comprised principally of electron density located on the ligand atoms, ~97% (Tables S2 and S3 in the SI). This explains its weak intensity, and, in fact, the transition draws its oscillator strength via a small amount of mixing with the Cu 4p orbitals.

In contrast, the B feature corresponds to the excitations into molecular orbitals, which due to their proximity to the continuum are rather diffuse (Figure 6, upper inset), but contains a larger 4p (dipole-allowed) contribution. In fact, Tables S2 and S3 in the SI show that the important molecular orbitals for this transition contain ~11% Cu 4p density. In addition, the diffuse nature of the molecular orbitals, which is in agreement with the analysis using the shell-by-shell simulation (Figure S4 in the SI), confirms previous assignments[33] that this feature is a sensitive probe of the bonding environment.

**Excited State.** Having characterized the ground-state spectrum, we now turn to the $^3$MLCT state. Upon MLCT excitation, Cu(I) becomes Cu(II), which results in a blue shift of the edge in the excited state spectrum. To some extent it is possible to isolate this change by approximating the transient spectrum as an energy-shifted ground-state spectrum minus the original ground-state spectrum, and throughout the following text we refer to it as the *shifted difference* spectrum. This will clearly not give any structural information, but it is useful in characterizing the extent to which the changes in the transient spectrum can be attributed to the oxidation shift. Figure 7a shows the experimental transient and *shifted difference* spectrum, for which we have applied a 3 eV shift in accordance with the chemical shift derived by electrolysis.[32] The two difference spectra are normalized to the signal at 8.984 keV. The agreement between them is rather good given the simplicity of the analysis, showing that to a large extent the changes therein can be associated with the oxidation state change of the copper center. This is not entirely surprising because although the dihedral angle between the planes of the two dmp ligands is reduced by ~25° in the $^3$MLCT states, the changes in the bond lengths are small (Table 2). In particular and important in the context of this present work, Figure 7a shows that the agreement for the lower resonances, which form the pre-edge (A and B) features, is very good, suggesting that these changes are not associated with the copper atom becoming pentacoordinated.

For a more detailed interpretation, we concentrate on the pre-edge and edge regions, which are the most important in view of the previous interpretations.[19,32] Figure 7b compares the experimental transient (a zoom of Figure 3a) at 50 ps and the TD-DFT calculated transient, that is, the triplet minus the ground-state spectrum. The features present in the experimental transient are reproduced in terms of both energy and relative intensity. In particular, the positive A′ feature arises, as expected, from a transition into the electron hole at the HOMO created by photoexcitation (Table S4 in the SI).


dx.doi.org/10.1021/jp403751m | J. Phys. Chem. A 2013, 117, 4591−4601

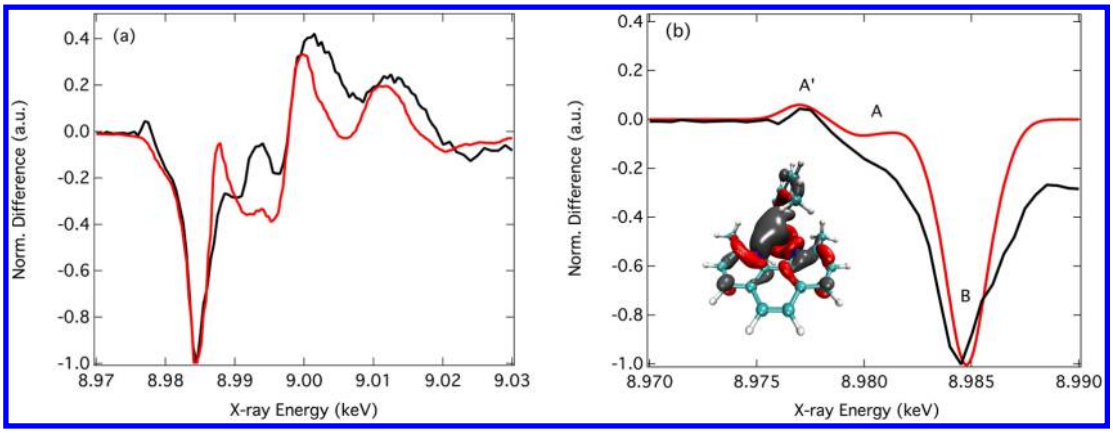


**Figure 7.** (a) Transient XANES spectrum of $[Cu(dmp)_2]^+$ dissolved in acetonitrile at 50 ps (black) and the shifted difference (red) of (ground state spectrum + 3 eV) minus ground state spectrum. (b) Simulated pre-edge transient spectrum (red, singlet minus triplet) using TD-DFT in comparison with the experimental transient (black). Inset is the molecular orbital for the transitions with the largest oscillator strengths for A′ (see also Tables S4 to S6).

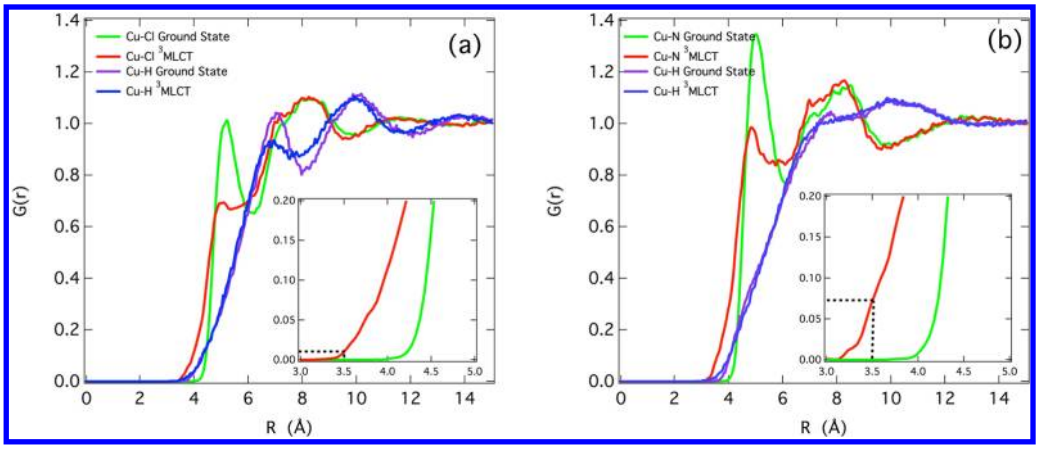


**Figure 8.** Classical MD trajectories simulations of: (a) Cu−Cl and Cu−H radial distribution functions for the ground and $^3$MLCT states of $[Cu(dmp)_2]^+$ in DCM and (b) Cu−$N_{MeCN}$ and Cu−$H_{MeCN}$ radial distribution functions for the ground and $^3$MLCT states of $[Cu(dmp)_2]^+$ dissolved in MeCN. The insets show a zoom of the $R$ < 5.0 Å region.

Because the HOMO is dominated by the Cu 3d-character, ∼60% (see Table S6 in the SI), this feature has previously been attributed to a 1s→3d quadrupole transition.[32,51] However, although the 3d orbitals give the largest contribution, there is a small contribution from the 4p density, which slightly increases upon the symmetry breaking structural changes in the $^3$MLCT state (Tables S3, S5, and S6 in the SI). As a consequence, this transition arises due to the dipole component, which is typically three orders of magnitude stronger than the corresponding quadrupole moment.[52,53]

The loss of the B feature, which was used as evidence of the exciplex formation,[19,32] is very well described by the simulation, even though the latter does not include the solvent. Just as for the shifted difference spectrum (Figure 7a), the loss of features A and B are associated with the blue shift due to the oxidation state change of the metal center. In the calculation, this is manifested by a lowering of the copper 1s orbital energy from 8.990 to 8.993 keV, as shown in Figure S5 in the SI. To further demonstrate the role of the oxidation shift, Figure S6 in the SI shows the calculated spectrum for the ground state and $^3$MLCT state at the ground state (perpendicular) and the flattened geometry. This shows that in the energy range of Figure 7b (8.970 to 8.987 keV), using either the perpendicular or flattened geometry for the $^3$MLCT state will yield almost identical transient spectra; consequently, the changes primarily originate from the change of oxidation state (Cu(I) to Cu(II)).

Finally, concerning the above-ionization resonances, which carry geometric information, Figure 7a shows, as previously mentioned, that these features can also to a certain extent be accounted for by the oxidation shift. However, there are deviations, particularly just above 8.99 keV, that are a consequence of the changes in the dmp-Cu-dmp dihedral angle in the $^3$MLCT state to which the XANES region is sensitive. Simulations of the transient spectrum, using the DFT(B3LYP) optimized ground and $^3$MLCT state geometries, were unable to account for these features. However, given that the transient spectra in MeCN and DCM are the same (Figure 3b), these deviations cannot be due to the solvent, and we attribute this to the approximations made in the phenomenological broadening, used to account for many body effects, which we discuss in more detail below.

## ■ MOLECULAR DYNAMICS SIMULATIONS

From the above, we can conclude that, if at all present, complexation with a solvent molecule at the metal atom is not visible on the transient XAS spectra. Therefore, solvent quenching of the photoluminescence must have another explanation. To investigate this further, we present hereafter


dx.doi.org/10.1021/jp403751m | J. Phys. Chem. A 2013, 117, 4591−4601

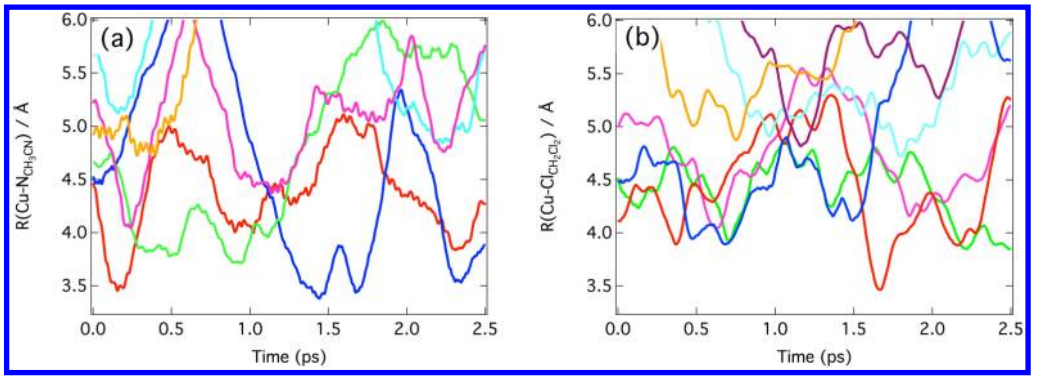


**Figure 9.** QM/MM MD of the lowest $^3$MLCT state of $[Cu(dmp)_2]^+$ in (a) MeCN (Cu−$N_{MeCN}$ distance) and (b) DCM (Cu−$Cl_{DCM}$). Each color represents a different solvent molecule that comes closer than 5 Å to the Cu.

CMD and QM/MM MD simulations of the ground and excited $[Cu(dmp)_2]^+$ in DCM and MeCN.

Figure 8a shows the radial distribution functions (RDFs) obtained by CMD of $[Cu(dmp)_2]^+$ in DCM for both the ground and lowest $^3$MLCT states. The ground-state Cu−$Cl_{DCM}$ distribution exhibits a peak centered around 5 Å, followed by a second broader solvent shell between 6.5 and 9 Å. While this second peak remains unchanged in the $^3$MLCT state, the first peak is lost and the distribution spreads to shorter distances. A similar behavior is also observed for the Cu−$N_{MeCN}$ distributions of $[Cu(dmp)_2]^+$ in MeCN (Figure 8b), except that the first peak is more distinct, in both cases pointing to a more ordered first solvation shell. The insets of Figure 8a,b zoom into the 3.0 Å < $R$ < 5.0 Å regions of the RDF and show that whereas the Cu−$N_{MeCN}$ and the Cu−$Cl_{DCM}$ probabilities at short range are very similar for the ground-state complex, there is a larger probability at shorter distances for the former in the $^3$MLCT state. Importantly, regarding the previous assignment of exciplex formation in the excited state, the residence time for solvent molecules at $R$ < 5 Å from the metal center, calculated using the method described in ref 54, was found to be 100 fs for both solvents, indicating that no exciplex is formed.

To investigate this aspect further, we use QM/MM MD to visualize the solvent molecules that come close to the complex. Figure 9a shows the Cu−$N_{MeCN}$ distance for the MeCN molecules, which comes within 5.0 Å from the copper atom during the last 2.5 ps trajectory of the QM/MM MD simulation. This shows, in close agreement with the CMD simulations, that solvent molecules come to between ∼3.5 and 4.0 Å of the copper, with only four events of closest encounter having a residence time of ∼100−200 fs. While statistical sampling from these simulations requires further trajectories, the latter show that although solvent molecules approach the copper atom, no bound exciplex is observed, confirming the analysis of the classical MD and the transient XAS (Figure 3). Figure 9b shows that in DCM the Cu−$Cl_{DCM}$ distances for the complex dissolved in DCM are typically larger (>4.0 Å) than those in MeCN, but these differences are due to the relative size of the two atoms (i.e., N and Cl).

The combination of CMD and QM/MM MD simulations presented in Figure 9 provides only information about the distance between the copper atom and the solvent molecules and confirms, in agreement with our transient XAS, that no exciplex is formed. To rationalize the quenching of the excited state, we must consider the electrostatic interaction energy between $[Cu(dmp)_2]^+$ and nearby (<5.0 Å) solvent molecules. Here the QM/MM MD simulations show that this increases by ∼0.3 eV between the ground and $^3$MLCT of $[Cu(dmp)_2]^+$ dissolved in MeCN, consistent with the more open structure due to the Jahn−Teller distortion of the complex. In contrast the electrostatic interaction energy with DCM increases by only 0.17 eV. This demonstrates, consistent with the emission data of refs 22 and 25 that a solvent interaction exists for both donating and nondonating solvents, but that in agreement with the fluorescence quenching and electron-donating properties, this effect, and therefore the solvent stabilization, is larger for the former.

## DISCUSSION

The above results demonstrate that: (i) The emission spectrum of $[Cu(dmp)_2]^+$ dissolved in MeCN is slightly (∼40 meV) red-shifted in comparison with DCM, pointing to a solvent stabilization of the lowest $^3$MLCT state. (ii) The transient X-ray absorption spectra of $[Cu(dmp)_2]^+$ are identical in MeCN and DCM solvents. For the former, they are also identical at 50 ps and 1 ns time delays. This rules out the formation of a pentacoordinated copper atom in the excited state, which was postulated for MeCN. (iii) Simulations of the experimental signals achieve good agreement with both the ground and transient spectra in the pre-edge and edge regions, using only the optimized geometry for the two states of interest without including the solvent.

We now discuss the optical emission spectra and the static and picosecond X-ray absorption spectra, paying particular attention to their implications on the structure, dynamics, and the effect of the solvent.

**Molecular Structure.** Table 2 summarizes the important structural parameters from this work. The DFT (B3LYP) optimized geometry of the ground state yields a Cu−N distance slightly larger than that of the EXAFS fit, which itself is in close agreement with the Cu−N bond distance extracted from the QM/MM MD trajectory. Importantly, the latter two are supported by the agreement between the experimental and simulated XANES spectra and the structure obtained by X-ray diffraction.[47,55] The N−Cu−N angle and the dihedral (flattening) between the dmp planes are found to be ∼83.5 and 89.75°, respectively, and are in agreement with the previous analysis of Chen et al.[19]

Upon photoexcitation and the subsequent ultrafast relaxation into the lowest $^3$MLCT state, we observe (using the DFT-optimized geometry) a contraction of the Cu−N bond by 0.08 Å, consistent with the removal of a d$\pi$ anti-bonding electron from the metal atom. The bond length of 2.0 Å agrees with the QM/MM MD but is smaller than the Cu−N distance reported


dx.doi.org/10.1021/jp403751m | J. Phys. Chem. A 2013, 117, 4591−4601

from the EXAFS fit of refs 19 and 32. However, in these cases, the bond distances were extracted using the excited-state EXAFS spectrum. This is a significant challenge due to limitations in signal-to-noise ratio, and, as a consequence, structural determination is prone to large uncertainties. The contraction of the Cu−N bond length induces a slight expansion of the N−Cu−N angle, which in the $^3$MLCT state increases by ∼2° to reach ∼83°.

Finally, the average value for the flattening angle (dmp-Cu-dmp) extracted from the DFT-optimized structure is similar to that obtained from the QM/MM MD and is ∼71°. This reduction plays an important role in the excited-state dynamics and the photoluminescence because it affects the magnitude of the spin orbit coupling. The angle presented here is ∼10° smaller than that reported by Chen et al.[19] but agrees with the flattening angle, which accounted for the blue shift in the excited state absorption spectrum in ref 18.

**X-ray Absorption Features.** Concerning the spectral features of the ground state K-edge spectra, extensive characterization of a variety of copper-containing complexes[33,56−58] has led to a detailed understanding of the ground-state spectrum. Our spectrum is in good agreement with these and previous studies of $[Cu(dmp)_2]^+$.[19,32,59] The TD-DFT simulations demonstrate, in agreement with these previous works, that the well-studied B feature predominately draws intensity from mixing with the 4p orbitals. In addition, our spectrum also exhibits a second, lower energy pre-edge feature, which, using TD-DFT, we are able to assign it to transitions into the LUMO and LUMO+1 orbitals.

The higher energy features, C and D, are above the edge. Feature D is, as demonstrated by the MS shell-by-shell analysis (Figure S4 in the SI), strongly influenced by the ligand structure farthest from the copper atom and bears many similarities to the resonances observed at the Fe K edge of $[Fe(bpy)]^{2+}$.[60] Although the agreement between experiment and theory for this feature is satisfactory, it is not as good as that for the lower energy features (Figure 6). In addition, simulations of the transient spectra, for which the Cu oxidation state is 2+, were unable to achieve a good agreement with experiment for the above ionization resonances in the range of the C and D features. These deviations likely originate from the description of many-body effects, accounted for using a phenomenological approach. It is interesting to note that Chaboy et al.[61] recently reported that these features in Cu(II) spectra are heavily influenced by multielectronic configurations and, in particular, are only correctly described only when two absorption channels are incorporated into the calculation. However, they used the MT approximation, which, as shown by Smolentsev et al.,[34,35] represents a significant approximation for this complex. We do not rule out multielectronic effects as a possible explanation for the deviation between the experiment and theory, but this is beyond the scope of the present work.

Turning to the excited state, the present transient XAS spectrum exhibits more details than previously reported,[34,35] primarily because of our high-repetition-rate pump−probe data acquisition scheme.[36] In the pre-edge region, we observe a relatively weak positive feature at ∼8.977 keV, which corresponds to a transition into the hole, created by photoexcitation, in the HOMO. This has been previously assigned as a 1s→3d transition.[32,51] This is supported by the fact that the important molecular orbital (see Tables S3, S5, and S6 in the SI) is dominated by Cu 3d density; however, there is a small amount of mixing between the 4p and 3d orbitals, and owing to the strength of dipole moments compared with quadrupole moments, the dipole contribution dominates. The previously described A and B features show up as negative features in the transient spectrum. Importantly, we demonstrate (Figure 7a) that these arise from the oxidation shift of the Cu atom (∼3 eV) and are not due to the formation of a pentacoordinated Cu atom. In summary, the X-ray absorption spectra of the excited complex in both solvents do not bear signatures of an exciplex formation reported in refs 19 and 32.

**Lifetime Quenching and the Solvent Effect.** Given that the fluorescence quenching is not due to the formation of a metal-centered exciplex, as previously reported, we must seek an alternative explanation. Toward this goal it is informative to consider a larger class of related complexes, presented in Table 1. These show, besides the solvent effect, distinct intramolecular effects,[62] as seen from the relative lifetimes of the different complexes in the same solvent. (See Figure S8 in the SI for the structures.) The luminescence properties of the Cu-phenanthrolines have previously been described in terms of a three-level system including emission from both the lowest $^1$MLCT and $^3$MLCT states, which are separated by ∼1800 $cm^{-1}$.[63] The $^1$MLCT state of $[Cu(dmp)_2]^+$ has a fluorescence lifetime of ∼13−16 ps;[45] therefore , the overall lifetime is determined by the longer lived $^3$MLCT state, which borrows intensity via the spin coupling with the $^1$MLCT state. The relationship between the fluorescence lifetime and the $^3$MLCT emission energy is demonstrated in Figure 10a, which shows the expected exponential behavior as a function of the energy gap between the ground and $^3$MLCT states.[24] Interestingly, although the majority of the complexes closely follow this curve, there are three distinct outliers: $[Cu(dpp)_2]^+$, $[Cu(dpdmp)_2]^+$, and $[Cu(tpp)_2]^+$. The first has a shorter lifetime than expected, while the latter two have a longer lifetime. The behavior of these complexes can be understood in terms of dihedral flattening of the emitting state and the energy gap between the $^1$MLCT and $^3$MLCT states. The optimized geometry of the $^3$MLCT state of $[Cu(dpp)_2]^+$ has a dihedral angle between the ligand planes of ∼82°, while for the latter two it is ∼62°, compared with ∼70−75° for most of the complexes. (See Table S10 in the SI). Siddique et al.[45] have reported that the spin−orbit coupling between the $^1$MLCT−$^3$MLCT decreases as a function of the dihedral angle; therefore, for small dihedral angles, the intensity borrowing from the $^1$MLCT will be large, and the phosphorescence lifetime is shortened. In contrast, for larger dihedral angles, this mixing is smaller, leading to longer lifetime. In addition, the efficiency of spin mixing between the two charge transfer states will also depend on the inverse of the energy gap between them,[45] and, as demonstrated in Table S11 in the SI, this gap is particularly small for $[Cu(dpp)_2]^+$, in contrast with the other Cu-phenanthrolines complexes. This will further increase the spin mixing between the two states and therefore the phosphorescence rate.

In terms of the solvent contribution, our CMD and QM/MM MD simulations of the solvent shell structure do not show evidence of exciplex formation in either DCM and MeCN. There is a small probability of solvent molecules coming to within 3.5 to 4 Å the copper atom, and the distance is smaller in MeCN. The residence time at the closest distance is between ∼100−200 fs before returning to the bulk. These QM/MM MD simulations have shown that a $[Cu(dmp)_2]^+$···solvent interaction exists for both donating and nondonating solvents;

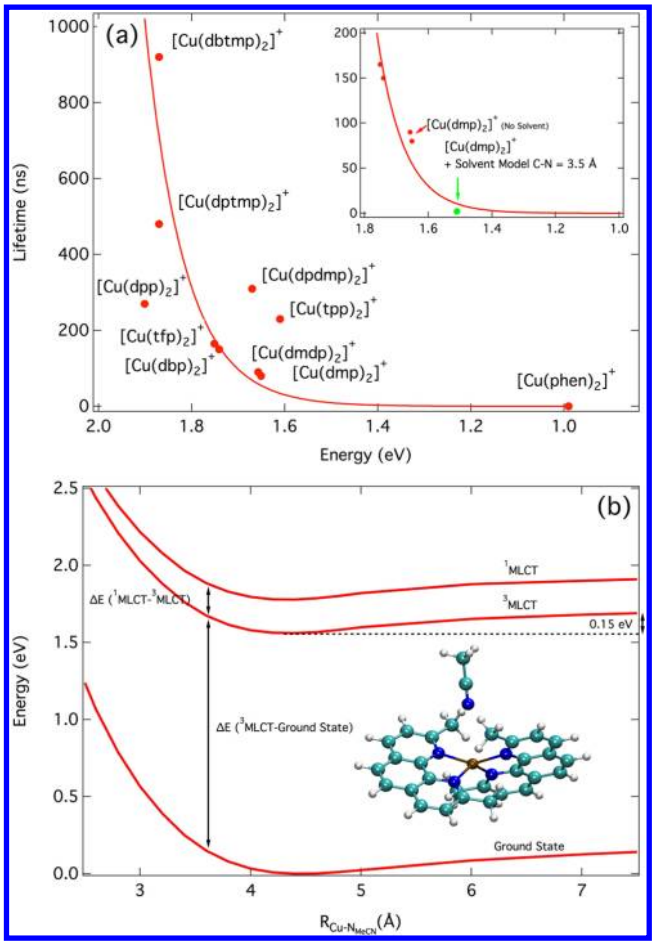


**Figure 10.** (a) Luminescence lifetime in DCM versus the calculated energy gap between the ground and $^3$MLCT states for 10 copper phenanthroline complexes. Inset is a zoom of the shorter lifetime complexes, including the experimental lifetime of $[Cu(dmp)_2]^+$ in MeCN and the calculated ground-state $^3$MLCT energy gap of the $[Cu(dmp)_2]^+$+solvent model. (b) DFT(B3LYP) and TDDFT-(B3LYP) calculated ground and lowest $^3$MLCT and $^1$MLCT states potential associated with the Cu−$N_{MeCN}$ distance. The structure of the complex when Cu−$N_{MeCN}$ = 3.5 Å is shown in the inset.

however, its increase (between the ground and $^3$MLCT states) is ∼0.13 eV larger for MeCN than for DCM. This is in agreement with the interaction energy, and resulting excited-state stabilization found using an geometry-optimized $[Cu(dmp)_2]^+\cdots CH_3CN$ adduct (Figure 10b). Plotting this energy gap (1.55 eV) and associated experimental lifetime on the exponential decay curve, shown in the inset in Figure 10a, we observe that this stabilization largely accounts for the quenching of the lifetime. The potential energy curves obtained by varying the Cu−$N_{MeCN}$ distance, shown in Figure 10b, demonstrate that the minimum of the potential in the $^3$MLCT state occurs around 4.2 Å; therefore, because the complex is on the repulsive part of the potential when Cu−$N_{MeCN}$ = 3.5 Å, it is not stable, and as demonstrated in the QM/MM MD simulations, the residence time of this complex would be expected to be small.

Finally, it is interesting to note that for our calculation of the energy gap excluding the solvent, the experimental lifetime lies just above the exponential curve (Figure 10a), while for the $[Cu(dmp)_2]^+$ + solvent model it lies below it. This is because although the solvent molecule reduces the energy gap between the ground and $^3$MLCT states, it also slightly reduces the gap between the $^3$MLCT and $^1$MLCT states, especially when Cu−$N_{MeCN}$ < 4.0 Å (Figure 10b). This will increase the mixing between the states, as previously discussed for $[Cu(dpp)_2]^+$, and therefore increase the phosphorescence rate. Although this is a rather fine effect, its influence could be important when considering the solvent quenching for related complexes.

## CONCLUSIONS

The present study aimed at shedding new light into the solvent effect on the photoluminescence quenching of excited $[Cu(dmp)_2]^+$ by means of static and time-resolved XAS, with a detailed theoretical analysis. Contrary to previous claims, the excited-state XAS spectra do not show evidence of the exciplex formation at the metal center that was invoked to explain the luminescence quenching. This is confirmed using MD simulations, which indicate only a weak interaction between the Cu and the solvent, as shown by the distance between the two, which is ∼3.5 to 4 Å. The strength of this interaction is comparable to a weak hydrogen bond and therefore, it undergoes rapid exchanges with the bulk solvent.

We have rationalized the lifetimes and solvent-dependent quenching of $[Cu(dmp)_2]^+$ in terms of the energy gap between the ground and $^3$MLCT states. The lifetime also depends on the spin−orbit-coupling, which itself is affected by the dihedral angle, and on the energy gap between the $^1$MLCT and $^3$MLCT states, and while its effect for this present complex is relatively small, it will likely have an important role for related Cu-phenanthrolines.

The picture that emergnes for Cu-phenanthrolines is that whereas previous modifications of the complex have focused on the substitution of bulky ligands to protect the metal center from interaction with the solvent species in the $^3$MLCT state, it is important to bear in mind that these modifications affect the torsional motion of the complex. This motion reduces the spin−orbit coupling and therefore the mixing of the $^1$MLCT and $^3$MLCT states, which lengthens the lifetime of the $^3$MLCT state.

## ASSOCIATED CONTENT

### Supporting Information

Methods and theory and computations. This material is available free of charge via the Internet at http://pubs.acs.org.

## AUTHOR INFORMATION

### Corresponding Author

*E-mail: majed.chergui@epfl.ch.

### Present Addresses

[⊥]F. A. Lima: Centro Nacional de Pesquisa em Energia e Materiais Laboratório Nacional de Luz Síncrotron Rua Giuseppe Máximo Scolfaro, 1000 13083-970 - Campinas, SP Brazil.

[#]C. J. Milne: SwissFEL, Paul Scherrer Inst, CH-5232 Villigen, CH.

### Notes

The authors declare no competing financial interest.

## ACKNOWLEDGMENTS

This work was funded in part by the Swiss NSF through the NCCR MUST 'Molecular ultrafast science and technology' and by contracts 200020-127231 and 200020-135502 and by the

COST action CM0701. We thank D. Grolimund and C. Borca for assistance during the measurements.

## REFERENCES

(1) Weaver, M. Dynamical Solvent Effects on Activated Electron-Transfer Reactions: Principles, Pitfalls, And Progress. *Chem. Rev.* **1992**, *92*, 463−480.
(2) de Boeij, W.; Pshenichnikov, M.; Wiersma, D. Ultrafast Solvation Dynamics Explored by Femtosecond Photon Echo Spectroscopies. *Annu. Rev. Phys. Chem.* **1998**, *49*, 99−123.
(3) Maroncelli, M. The Dynamics of Solvation in Polar Liquids. *J. Mol. Liq.* **1993**, *57*, 1−37.
(4) Ohtaki, H.; Radnai, T. Structure and Dynamics of Hydrated Ions. *Chem. Rev.* **1993**, *93*, 1157−1204.
(5) Bressler, C.; et al. Femtosecond XANES Study of the Light-Induced Spin Crossover Dynamics in an Iron(II) Complex. *Science* **2009**, *323*, 489−492.
(6) Bressler, C.; Chergui, M. Molecular Structural Dynamics Probed by Ultrafast X-Ray Absorption Spectroscopy. *Annu. Rev. Phys. Chem.* **2010**, *61*, 263−282.
(7) Chen, L. Probing Transient Molecular Structures in Photochemical Processes Using Laser-Initiated Time-Resolved X-ray Absorption Spectroscopy. *Annu. Rev. Phys. Chem.* **2005**, *56*, 221−254.
(8) Penfold, T.; Milne, C.; Chergui, M. Recent Advances in Ultrafast X-Ray Absorption Spectroscopy of Solutions. *Adv. Chem. Phys.* **2013**, *153*, 1−41.
(9) Pham, V.; et al. Probing the Transition from Hydrophilic to Hydrophobic Solvation with Atomic Scale Resolution. *J. Am. Chem. Soc.* **2011**, *133*, 12740−12748.
(10) El Nahhas, A.; et al. X-ray Absorption Spectroscopy of Ground and Excited Rhenium-Carbonyl-Diimine: Evidence for a Two-Center Electron Transfer. *J. Phys. Chem. A* **2013**, *117*, 361−369.
(11) Penfold, T.; Curchod, B.; Tavernelli, I.; Abela, R.; Rothlisberger, U.; Chergui, M. Simulations of X-ray Absorption Spectra: The Effect of the Solvent. *Phys. Chem. Chem. Phys.* **2012**, *14*, 9444−9450.
(12) McMillin, D.; Kirchhoff, J.; Goodwin, K. Exciplex Quenching of Photoexcited Copper Complexes. *Coord. Chem. Rev.* **1985**, *64*, 83−92.
(13) Blaskie, M.; McMillin, D. Photostudies of Copper(I) Systems. 6. Room-Temperature Emission and Quenching Studies of Bis(2,9-dimethyl-1,10-phenanthroline)copper(I). *Inorg. Chem.* **1980**, *19*, 3519−3522.
(14) Del Paggio, A.; McMillin, D. Substituent Effects and the Photoluminescence of Cu(PPh3)2(NN)+ Systems. *Inorg. Chem.* **1983**, *22*, 691−692.
(15) Armaroli, N. Photoactive Mono- and Polynuclear Cu (I)−phenanthrolines. A Viable Alternative to Ru (II)−polypyridines? *Chem. Soc. Rev.* **2001**, *30*, 113−124.
(16) Scaltrito, D.; Thompson, D.; O'Callaghan, J.; Meyer, G. MLCT Excited States of Cuprous Bis-Phenanthroline Coordination Compounds. *Coord. Chem. Rev.* **2000**, *208*, 243−266.
(17) Zgierski, M. Cu(I)-2,9-Dimethyl-1,10-phenanthroline: Density Functional Study of the Structure, Vibrational Force-Field, And Excited Electronic States. *J. Chem. Phys.* **2003**, *118*, 4045.
(18) Shaw, G.; Grant, C.; Shirota, H.; Castner, E.; Meyer, G.; Chen, L. Ultrafast Structural Rearrangements in the MLCT Excited State for Copper(I) Bis-Phenanthrolines in Solution. *J. Am. Chem. Soc.* **2007**, *129*, 2147−2160.
(19) Chen, L.; Shaw, G.; Novozhilova, I.; Liu, T.; Jennings, G.; Attenkofer, K.; Meyer, G.; Coppens, P. MLCT State Structure and Dynamics of a Copper(I) Diimine Complex Characterized by Pump-Probe X-ray and Laser Spectroscopies and DFT Calculations. *J. Am. Chem. Soc.* **2003**, *125*, 7022−7034.
(20) Iwamura, M.; Takeuchi, S.; Tahara, T. Real-Time Observation of the Photoinduced Structural Change of Bis(2,9-dimethyl-1,10-phenanthroline)copper(I) by Femtosecond Fluorescence Spectroscopy: A Realistic Potential Curve of the Jahn-Teller Distortion. *J. Am. Chem. Soc.* **2007**, *129*, 5248−5256.
(21) Iwamura, M.; Watanabe, H.; Ishii, K.; Takeuchi, S.; Tahara, T. Coherent Nuclear Dynamics in Ultrafast Photoinduced Structural Change of Bis(diimine) Copper (I) Complex. *J. Am. Chem. Soc.* **2011**, *133*, 7728.
(22) Eggleston, M.; McMillin, D.; Koenig, K.; Pallenberg, A. Steric Effects in the Ground and Excited States of Cu (NN) 2+ Systems. *Inorg. Chem.* **1997**, *36*, 172−176.
(23) Palmer, C.; McMillin, D.; Kirmaier, C.; Holten, D. Flash Photolysis and Quenching Studies of Copper (I) Systems in the Presence of Lewis Bases: Inorganic Exciplexes? *Inorg. Chem.* **1987**, *26*, 3167−3170.
(24) Englman, R.; Jortner, J. The Energy Gap Law for Radiationless Transitions in Large Molecules. *Mol. Phys.* **1970**, *18*, 145−164.
(25) Cunningham, C.; Cunningham, K.; Michalec, J.; McMillin, D. Cooperative Substituent Effects on the Excited States of Copper Phenanthrolines. *Inorg. Chem.* **1999**, *38*, 4388−4392.
(26) Gothard, N.; Mara, M.; Huang, J.; Szarko, J.; Rolczynski, B.; Lockard, J.; Chen, L. Strong Steric Hindrance Effect on Excited State Structural Dynamics of Cu(I) Diimine Complexes. *J Phys. Chem. A* **2012**, *116*, 1984−1992.
(27) Lockard, J.; et al. Triplet Excited State Distortions in a Pyrazolate Bridged Platinum Dimer Measured by X-ray Transient Absorption Spectroscopy. *J. Phys. Chem. A* **2010**, *114*, 12780.
(28) Lockard, J.; Kabehie, S.; Zink, J.; Smolentsev, G.; Soldatov, A.; Chen, L. Influence of Ligand Substitution on Excited State Structural Dynamics in Cu(I) Bisphenanthroline Complexes. *J. Phys. Chem. B* **2010**, *114*, 14521−14527.
(29) Gutmann, V. Ion-Pairing and Outer Sphere Effect. *Chimia* **1977**, *31*, 1−7.
(30) Ichinaga, A.; Kirchhoff, J.; McMillin, D.; Dietrich-Buchecker, C.; Marnot, P.; Sauvage, J. Charge-Transfer Absorption and Emission of Cu (NN) 2+ Systems. *Inorg. Chem.* **1987**, *26*, 4290−4292.
(31) Eggleston, M.; Fanwick, P.; Pallenberg, A.; McMillin, D. A Twist on the Copper Center in the Crystal Structure of [Cu(dnpp)2]PF6 and the Charge-Transfer Excited State? (dnpp = 2,9-Dineopentyl-1,10-phenanthroline). *Inorg. Chem.* **1997**, *36*, 4007−4010.
(32) Chen, L. X.; Jennings, G.; Liu, T.; Gosztola, D.; Hessler, J.; Scaltrito, D.; Meyer, G. Rapid Excited-State Structural Reorganization Captured by Pulsed X-rays. *J. Am. Chem. Soc.* **2002**, *124*, 10861−10867.
(33) Kau, L.; Spira-Solomon, D.; Penner-Hahn, J.; Hodgson, K.; Solomon, E. X-ray Absorption Edge Determination of the Oxidation State and Coordination Number of Copper: Application to the Type 3 Site in Rhus vernicifera Laccase and Its Reaction with Oxygen. *J. Am. Chem. Soc.* **1987**, *109*, 6433.
(34) Smolentsev, G.; Soldatov, A.; Chen, L. Three-Dimensional Local Structure of Photoexcited Cu Diimine Complex Refined by Quantitative XANES Analysis. *J. Phys. Chem. A* **2008**, *112*, 5363−5367.
(35) Smolentsev, G.; Sukharina, G.; Soldatov, A.; Chen, L. X. Application of XANES Spectroscopy to Study Local Structure of Photoexcited Cu Complex. *Nucl. Instrum. Methods Phys. Res., Sect. A* **2009**, *603*, 122−124.
(36) Lima, F.; et al. a High-Repetition Rate Scheme for Synchrotron-Based Picosecond Laser Pump/X-ray Probe Experiments on Chemical and Biological Systems in Solution. *Rev. Sci. Instrum.* **2011**, *82*, 063111.
(37) Joly, Y. X-ray Absorption near-Edge Structure Calculations beyond the Muffin-Tin Approximation. *Phys. Rev. B* **2001**, *63*, 1−10.
(38) DeBeer-George, S.; Petrenko, T.; Neese, F. Prediction of Iron K-Edge Absorption Spectra Using Time-Dependent Density Functional Theory. *J. Phys. Chem. A* **2008**, *112*, 12936−12943.
(39) Debeer-George, S.; Petrenko, T.; Neese, F. Time-Dependent Density Functional Calculations of Ligand K-edge X-ray Absorption Spectra. *Inorg. Chim. Acta* **2008**, *361*, 965−972.
(40) Neese, F.; Becker, U.; Ganyushin, D.; Kossmann, S.; Hansen, A.; Liakos, D.; Petrenko, T.; Riplinger, C.; Wennmohs, F. *ORCA - An Ab Initio, Density Functional and Semiempirical Program Package*; Max Planck Institute for Bioinorganic Chemistry: Mulheim, Germany, 2012.
(41) Rothlisberger, U.; Carloni, P. Drug-Target Binding Investigated by Quantum Mechanical/Molecular Mechanical (QM/MM) Methods. *Lect. Notes Phys.* **2006**, *704*, 437−466.

(42) Laio, A.; VandeVondele, J.; Rothlisberger, U. D-RESP: Dynamically Generated Electrostatic Potential Derived Charges from Quantum Mechanics/Molecular Mechanics Simulations. *J. Phys. Chem. B* **2002**, *106*, 7300−7307.
(43) Laio, A.; VandeVondele, J.; Rothlisberger, U. A Hamiltonian Electrostatic Coupling Scheme for Hybrid Car-Parrinello Molecular Dynamics Simulations. *J. Chem. Phys.* **2002**, *116*, 6941−6947.
(44) Pham, V.; Tavernelli, I.; Milne, C.; van der Veen, R.; D'Angelo, P.; Bressler, C.; Chergui, M. The Solvent Shell Structure of Aqueous Iodide: X-ray Absorption Spectroscopy and Classical, Hybrid QM/MM and Full Quantum Molecular Dynamics Simulations. *Chem. Phys.* **2010**, *371*, 24−29.
(45) Siddique, Z.; Yamamoto, Y.; Ohno, T.; Nozaki, K. Structure-Dependent Photophysical Properties of Singlet and Triplet Metal-to-Ligand Charge Transfer States in Copper(I) Bis(diimine) compounds. *Inorg. Chem.* **2003**, *42*, 6366−6378.
(46) Newville, M. IFEFFIT: Interactive XAFS Analysis and FEFF Fitting. *J. Synchrotron Radiat.* **2001**, *8*, 322−324.
(47) King, G.; Gembicky, M.; Coppens, P. Two Novel Bis(2,9-dimethyl-1,10-phenanthroline)copper(I) Complexes: [Cu(dmp)2]2-(PF6)2.0.5(bpmh).CH3CN and [Cu(dmp)2][N(CN)2]. *Acta Crystallogr., Sect. C: Cryst. Struct. Commun.* **2005**, *61*, 1−4.
(48) Kovalevsky, A.; Gembicky, M.; Coppens, P. Cu (I)(2,9-Bis(trifluoromethyl)-1,10-phenanthroline) 2+Complexes: Correlation between Solid-State Structure and Photoluminescent Properties. *Inorg. Chem.* **2004**, *43*, 8282−8289.
(49) Briois, V.; Sainctavit, P.; Long, G. J.; Grandjean, F. Importance of Photoelectron Multiple Scattering in the Iron K-edge X-ray Absorption Spectra of Spin-Crossover Complexes: Full Multiple Scattering Calculations for Several Iron(II) Trispyrazolylborate and Trispyrazolylmethane Complexes. *Inorg. Chem.* **2001**, *40*, 912−918.
(50) Krause, M.; Oliver, J. H. Natural Widths of Atomic K and L Levels, Ka X-ray Lines and Several KLL Auger Lines. *J. Phys. Chem. Ref. Data* **1979**, *8*, 329−338.
(51) Shulman, G. R.; Yafet, Y.; Eisenberger, P.; Blumberg, W. E. Observations and Interpretation of X-Ray Absorption Edges in Iron Compounds and Proteins. *Proc. Natl. Acad. Sci.* **1976**, *73*, 1384.
(52) Yamamoto, T. Assignment of Pre-Edge Peaks in K-edge X-ray Spectra of 3d Transition Metal Compounds: Electric Dipole or Quadrupole? *X-Ray Spectrom.* **2008**, *37*, 572−584.
(53) Westre, T.; Kennepohl, P.; DeWitt, J.; Hedman, B.; Hodgson, K.; Solomon, E. A Multiplet Analysis of Fe K-Edge 1s-3d Pre-Edge Features of Iron Complexes. *J. Am. Chem. Soc.* **1997**, *119*, 6297−6314.
(54) Moret, M.-E.; Tavernelli, I.; Rothlisberger, U. Combined QM/MM and Classical Molecular Dynamics Study of [Ru(bpy)(3)](2+) in Water. *J. Phys. Chem. B* **2009**, *113*, 7737−7744.
(55) Vorontsov, I.; Graber, T.; Kovalevsky, A.; Novozhilova, I.; Gembicky, M.; Chen, Y.-S.; Coppens, P. Capturing and Analyzing the Excited-State Structure of a Cu(I) Phenanthroline Complex by Time-Resolved Diffraction and Theoretical Calculations. *J. Am. Chem. Soc.* **2009**, *131*, 6566−6573, PMID: 19378949.
(56) Frank, P.; Benfatto, M.; Hedman, B.; Hodgson, K. O. Solution [Cu(amm)] 2+is a Strongly Solvated Square Pyramid: A Full Account of the Copper K-edge XAS Spectrum Within Single-Electron Theory. *Inorg. Chem.* **2008**, *47*, 4126−4139.
(57) Shadle, S.; Hedman, B.; Hodgson, K.; Solomon, E. Ligand K-Edge X-ray Absorption Spectroscopy as a Probe of Ligand-Metal Bonding: Charge Donation and Covalency in Copper-Chloride Systems. *Inorg. Chem.* **1994**, *33*, 4235−4244.
(58) Solomon, E.; Szilagyi, R.; DeBeer George, S.; Basumallick, L. Electronic Structures of Metal Sites in Proteins and Models: Contributions to Function in Blue Copper Proteins. *Chem. Rev.* **2004**, *104*, 419−458.
(59) Mesu, J.; Beale, A.; de Groot, F.; Weckhuysen, B. Probing the Influence of X-rays on Aqueous Copper Solutions Using Time-Resolved in Situ Combined Video/X-ray Absorption near-Edge/Ultraviolet-Visible Spectroscopy. *J. Phys. Chem. B* **2006**, *110*, 17671−17677.
(60) Gawelda, W.; Pham, V. T.; van der Veen, R. M.; Grolimund, D.; Abela, R.; Chergui, M.; Bressler, C. Structural Analysis of Ultrafast Extended X-ray Absorption Fine Structure with Subpicometer Spatial Resolution: Application to Spin Crossover Complexes. *J. Chem. Phys.* **2009**, *130*, 124520.
(61) Chaboy, J.; Muñoz-Páez, A.; Carrera, F.; Merkling, P.; Marcos, E. Ab Initio X-ray Absorption Study of Copper K-edge XANES Spectra in Cu (II) Compounds. *Phys. Rev. B* **2005**, *71*, 134208.
(62) Felder, D.; Nierengarten, J.; Barigelletti, F.; Ventura, B.; Armaroli, N. Highly Luminescent Cu(I)-Phenanthroline Complexes in Riatrix and Temperature Dependence of the Photophysical Properties. *J. Am. Chem. Soc.* **2001**, *123*, 6291−6299.
(63) Kirchhoff, J.; Gamache, R., Jr.; Blaskie, M.; Del Paggio, A.; Lengel, R.; McMillin, D. Temperature Dependence of Luminescence from Cu (NN) 2+ Systems in Fluid Solution. Evidence for the Participation of Two Excited States. *Inorg. Chem.* **1983**, *22*, 2380−2384.